Controlling surface defect valence in colloids

G. Skačej[1] and C. Zannoni[2]

[1] *Fakulteta za matematiko in fiziko, Univerza v Ljubljani, Jadranska 19, SI-1000 Ljubljana, Slovenia*
[2] *Dipartimento di Chimica Fisica ed Inorganica and INSTM - CRIMSON,*
Università di Bologna, Viale Risorgimento 4, I-40136 Bologna, Italy
(Dated: March 15, 2008)

We perform large-scale Monte Carlo simulations of orientational ordering in nematic shells and study the type and position of topological defects when an external electric field (homogeneous or quadrupolar) is applied. The field-induced variation of the defect number (and strength) can be used to change the valence of colloidal particles coated with a nematic layer.

In a seminal paper of only a few years ago, Nelson [1] suggested the fascinating possibility of doing chemistry using colloidal particles coated with a layer of liquid crystals, rather than atoms. Theoretically, upon covering a micro-size sphere with a thin layer of nematic liquid crystal — characterized by a quadrupolar symmetry order parameter — four half-strength topological defects [2] are predicted, consistently with the Poincaré constraint that the total surface defect charge should in this case equal 2 [1, 3]. These defects, placed at the vertices of a regular tetrahedron, represent high-free energy spots, potentially suitable for a chemical attack, so as to build complex colloidal architectures [4, 5], e.g., for photonic applications. Various alternative strategies for decorating nanoparticles have recently been proposed, e.g., via nanoembossing by metal vapor deposition on colloidal crystals [6], by grafting binary polymer brushes [7], and via micro and nanosize spherical particle binary dispersions in oil-in-water emulsion droplets [8]. However, colloidal defects creation seems to be a particularly elegant and potentially powerful method. Experimentally, the first such systems — nematic layer-covered microdroplets — have been prepared using microfluidic techniques [9, 10]. Alternatively, tetrahedral defect configurations have been predicted for the nematic wetting layers surrounding a spherical particle with planar anchoring [12]. It might then become possible to create three-dimensional architectures where high-free energy defect cores are used as attachment points for complex linkers such as deoxyribonucleic acid or polymer linkers [1, 11]. In this perspective it seems very important to have the possibility of controlling the coordination number and the valence angles of the "colloidal atoms" by changing the number of surface defects and/or their position on the spherical particle. For nematic shells it has been predicted that two rather than four surface defects should be obtained in the case of a polar nematic [1], but this does not seem a viable route towards inducing a valence change, as polar fluid liquid crystals have not been found as yet. Here we are exploring the possibility, that should be accessible to experiment, of controlling the defect locations by applying an external (e.g., electric) field, either uniform or

with a specific multipolar character. Our study is based on lattice Monte Carlo (MC) simulations, instead of applying purely theoretical arguments, because on one hand we can show — where comparison is possible — that the two treatments give the same results while, at the same time, the simulation approach offers a greater flexibility for the variety of cases we wish to consider.

We have performed large-scale MC simulations of liquid-crystalline ordering in spherical nematic shells, based on the Lebwohl-Lasher (LL) lattice model [13] consisting of a system of N rotors/particles $\mathbf{u}_i$ (unit vectors representing close-packed clusters of $\sim 10^2$ nematogenic molecules) positioned at the nodes of a simple cubic lattice with spacing a. The LL Hamiltonian is given by $\mathcal{H}_n = -\sum_{\langle ij \rangle} \epsilon_{ij} P_2(\mathbf{u}_i \cdot \mathbf{u}_j)$, where the sum runs over nearest neighbors $\mathbf{u}_i$ and $\mathbf{u}_j$ only, ϵ_{ij} is a constant, and $P_2(x) = (3x^2 - 1)/2$. In the bulk one has $\epsilon_{ij} = \epsilon > 0$. Then $\mathcal{H}_n$ favors parallel alignment of nearest-neighbor particles, compatibly with the imposed boundary conditions. It has already been demonstrated that LL simulations can be used to study topological defects in thin liquid crystal films [14]. Here, however, our sample was comprised between two concentric spheres carved from the cubic lattice, with the inner and outer sphere radii set to $30a$ and $40a$, respectively, yielding a total of $N = 148968$ shell particles. Tangential (planar degenerate) boundary conditions at both surfaces were imposed by an additional layer of "ghost" particles, fixed along the radial direction from the common sphere center, with $\epsilon_{ij} = -\epsilon < 0$ for the ghost-nematic interaction. (This corresponds to strong planar anchoring.) Finally, the aligning effect of the external electric field was modeled by $\mathcal{H}_f = -\epsilon\eta \sum_{i=1}^{N} F_i^2 P_2(\mathbf{u}_i \cdot \mathbf{f}_i)$, where η is a field coupling term proportional also to the dielectric anisotropy ϵ_a. For $\epsilon_a > 0$ particle long axes $\mathbf{u}_i$ are aligned along the local field $\mathbf{F}_i = F_i\mathbf{f}_i$, where $\mathbf{f}_i$ is a unit vector and $F_i = |\mathbf{F}_i|$. Hence, in an inhomogeneous field the alignment coupling strength is spatially-dependent and is locally given by $\epsilon\eta F_i^2$.

Our MC runs were performed for $T^* = k_B T/\epsilon = 1.0$, i.e., well below the bulk nematic-isotropic transition temperature $T_{NI}^* \approx 1.1232$ [15], increasing and decreasing
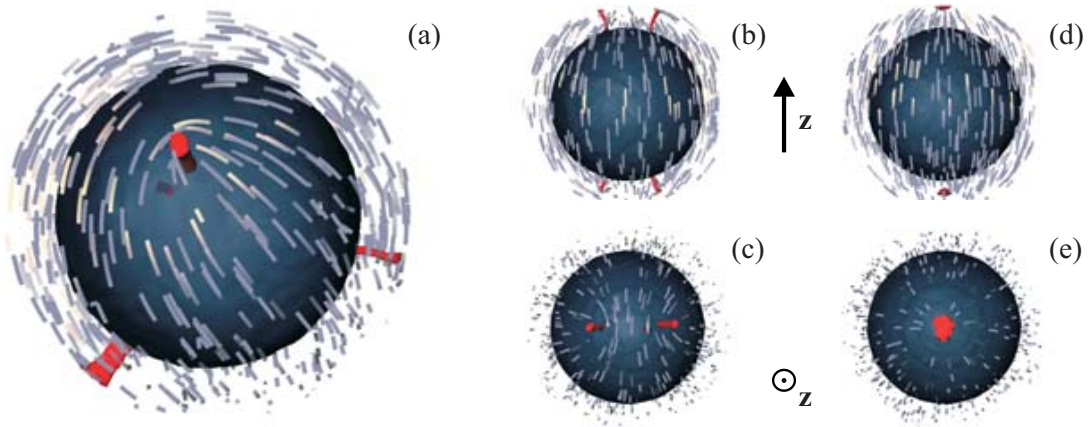
FIG. 1: (color online) Nematic shell: director field and defect positions in absence of external field (a), and in a homogeneous field directed along $\mathbf{z}$, with $\eta = 0.03$ (b,c) and $\eta = 0.06$ (d,e). View perpendicular to $\mathbf{z}$ (b,d) and along $\mathbf{z}$ (c,e). The defects are indicated by red color, the director field by streamlines. The dark sphere represents the inner shell surface; the outer shell is not shown.

the external field strength. Trial moves — attempted particle rotations [16], in a random sequence [15] — were accepted/rejected following the Metropolis algorithm [17], while maintaining the acceptance ratio close to 50%. Each run was started from the configuration equilibrated at the nearest lower/higher value of η; then 280 MC kcycles (a cycle equals N attempted MC moves) were performed for equilibration, followed by 20 MC kcycles for production. To visualize nematic director fields, we followed Callan-Jones et al. [18], calculating the average components of the local ordering matrix $\mathsf{U}_i = \langle \mathbf{u}_i \otimes \mathbf{u}_i \rangle$ for each lattice site. (Here $\langle \cdots \rangle$ denotes an average over MC cycles.) Then, U_i was diagonalized, yielding the eigenvalues $\lambda_1^i \geq \lambda_2^i \geq \lambda_3^i$, as well as the corresponding eigenvectors. The local director was identified as the eigenvector corresponding to λ_1^i. The nature of nematic ordering can be presented in terms of the three Westin metrics: $c_l^i = \lambda_1^i - \lambda_2^i$, $c_p^i = 2(\lambda_2^i - \lambda_3^i)$, and $c_s^i = 3\lambda_3^i$ [18]. Then, $c_l^i \approx 1$ is a signature of a well-ordered uniaxial nematic, $c_p^i \approx 1$ corresponds to pronounced planar ordering, and $c_s^i \approx 1$ to isotropy (no ordering). Topological defects are characterized by absence of pronounced uniaxial ordering and can therefore be identified as regions where c_l drops below a certain threshold. As in [18] we here used $c_l^i < 0.12$, unless noted otherwise. The defect strength — surface topological charge — is determined from the calculated director fields by monitoring the director rotation along a closed loop enclosing the defect on the inner/outer shell surface [19, 20].

Turning now to the results, we observe first, in the absence of an external electric field, a director configuration with four defect lines penetrating the shell, with a strength $s = 1/2$, as predicted for one elastic constant curvature elasticity in Ref. [1]. (Note that using the LL model actually corresponds to working in the

one-constant approximation.) The corresponding director field is shown in Fig. 1 (a). The repulsion between defect lines maximizes the line-to-line distance, therefore the lines are located approximately at the vertices of a tetrahedron, its orientation in space being degenerate. We have observed that this changes once the inner and outer spheres are not concentric anymore, as, e.g., due to effects of gravity in a real experiment: our simulations show that the defect lines then move towards the thinner part of the shell to reduce their length, which agrees with the observations of Ref. [10]. The diameter of the defect line core is estimated as $6a$ approximately, which is compatible with the estimate for the nematic correlation length in the LL model. If the average production period is extended too much, the image of the defects is smeared out since they fluctuate around their equilibrium positions, as suggested in Ref. [1].

It has been predicted that the four-defect line tetrahedral configuration is stable only in rather thin shells. Instead, in thick shells a bipolar configuration should be observed, where the disclination lines are replaced by a three-dimensional escaped structure with surface point
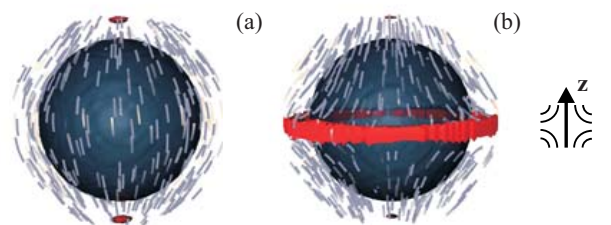

FIG. 2: (color online) Same as Fig. 1, however for a axially-symmetric quadrupolar F_i^0-type external field (depicted schematically as inset) for $\eta = 0.045$ (a) and $\eta = 0.18$ (b). The field symmetry axis is parallel to $\mathbf{z}$, the c_l threshold equals 0.24.
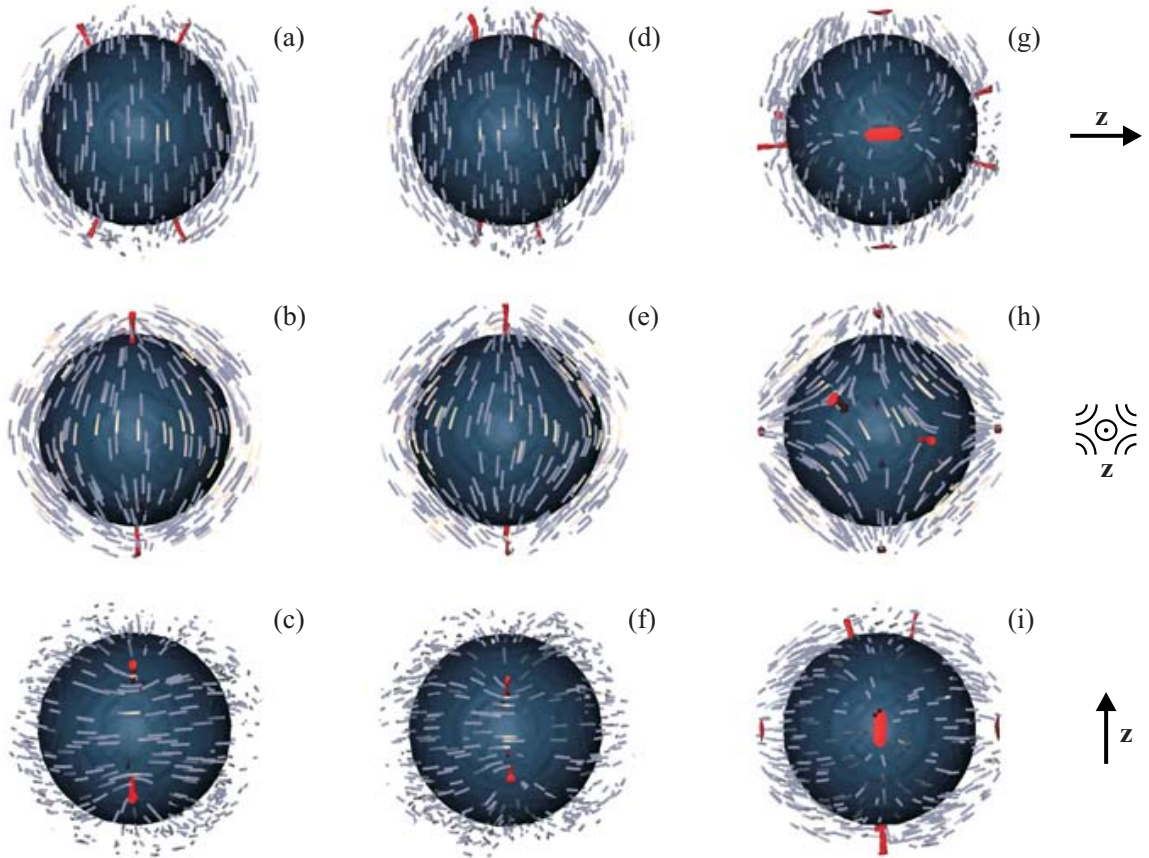
FIG. 3: (color online) Same as Fig. 2, however for a quadrupolar F_i^2-type field, as seen from three mutually perpendicular directions. Field cross section normal to **z** and z-axis orientations are shown schematically as insets; $\eta = 0.015$ (a-c), $\eta = 0.03$ (d-f), and $\eta = 0.05$ (g-i).

defects at the shell surface poles [9, 21]. Therefore, we have also performed some simulation runs varying the inner sphere radius, and the four-defect line configuration turns out to be stable for radii above $\sim 12a$. The three-defect line configurations seen experimentally [10] have not been observed so far. — Moreover, we have performed some testing runs with a Heisenberg model-like P_1-type (polar) inter-particle potential in a shell, observing a pair of $s = 1$ defects at the shell poles [1].

Let us now consider a nematic shell exposed to a homogeneous external electric field along the z-axis, taking $\mathbf{F}_i = (0, 0, 1)$. In the following we assume, for simplicity, that the dielectric anisotropy of the nematic is not extremely large so that the local direction and strength of the external field are not affected by the local ordering of the nematic material. (In the opposite case a self-consistent solution of Maxwell equations would be necessary during the MC evolution.) Then, in a typical nematic $\eta = 0.1$ corresponds to a field strength of ~ 30 V/μm [22]. The gradual evolution of the defect line position on the sphere can be deduced from Fig. 1 (b-e): on increasing the field strength, first the defect line tetrahedron deforms and aligns as required by the field, and finally the four $s = 1/2$ defect lines penetrating the shell

partially coalesce to form two pairs of $s = 1$ surface point defects at the inner/outer sphere poles [Fig. 1 (d,e)]. Here the bipolar axis is parallel to the field direction. Note that such escaped surface defects will typically be seen in a strong field wherever the field is directed along the local shell normal, thus being in conflict with surface boundary conditions. — At this point we have succeeded in changing the colloidal valence from 4 to 2. During this process the surface topological defect charge remained constant and equal 2.

In order to further manipulate defects on a nematic shell, one can also use an inhomogeneous external field. In fact, inhomogeneous electric fields with multipolar character have already been implemented experimentally, e.g., in a spherical electrical charge-free area surrounded by electrodes [23]. In such a device, the first higher-order (i.e., quadrupolar) solution of the Poisson equation for the electrostatic potential can be written as $\phi(\mathbf{r}) = \sum_{m=-2}^{2} c_m \mathbf{r} \cdot \mathsf{Q}^m \mathbf{r}$ [24], where the Cartesian coordinates $\mathbf{r}$ are measured from the sphere center, c_m are constants and Q^m is the second-rank tensorial base given by $\mathsf{Q}^0 = (3\mathbf{e}_z \otimes \mathbf{e}_z - \mathsf{I})/\sqrt{6}$, $\mathsf{Q}^1 = (\mathbf{e}_x \otimes \mathbf{e}_z + \mathbf{e}_z \otimes \mathbf{e}_x)/\sqrt{2}$, $\mathsf{Q}^{-1} = (\mathbf{e}_y \otimes \mathbf{e}_z + \mathbf{e}_z \otimes \mathbf{e}_y)/\sqrt{2}$, $\mathsf{Q}^2 = (\mathbf{e}_x \otimes \mathbf{e}_x - \mathbf{e}_y \otimes \mathbf{e}_y)/\sqrt{2}$, and $\mathsf{Q}^{-2} = (\mathbf{e}_x \otimes \mathbf{e}_y + \mathbf{e}_y \otimes \mathbf{e}_x)/\sqrt{2}$. (Above $\mathbf{e}_x$, $\mathbf{e}_y$,

and $\mathbf{e}_z$ denote the orthonormal Cartesian triad, and I the identity matrix.) Then, the resulting electric field equals $\mathbf{E}(\mathbf{r}) = -\nabla\phi(\mathbf{r}) = -2\sum_{m=-2}^{2} c_m \mathsf{Q}^m \mathbf{r}$. Like for the homogeneous case, we have studied nematic ordering in a shell exposed to the five independent quadrupolar field components $\mathbf{E}^m(\mathbf{r}) = -2c_m \mathsf{Q}^m \mathbf{r}$. For the ith lattice site at $\mathbf{r}_i = (x_i, y_i, z_i)$ the corresponding local field vectors $\mathbf{F}_i^m \propto \mathbf{E}^m(\mathbf{r}_i)$ used in $\mathcal{H}_f$ become: $\mathbf{F}_i^0 = \sqrt{2/3}(x_i, y_i, -2z_i)/a$, $\mathbf{F}_i^1 = -\sqrt{2}(z_i, 0, x_i)/a$, $\mathbf{F}_i^{-1} = -\sqrt{2}(0, z_i, y_i)/a$, $\mathbf{F}_i^2 = \sqrt{2}(-x_i, y_i, 0)/a$, and $\mathbf{F}_i^{-2} = -\sqrt{2}(y_i, x_i, 0)/a$.

Let us first focus on the axially symmetric $\mathbf{F}_i^0$-type field enjoying $D_{\infty h}$ symmetry. At intermediate field strengths $\mathbf{F}_i^0$ produces patterns similar to those seen for the bipolar shell in the homogeneous field, with two pairs of $s = 1$ surface defects at the poles; see Fig. 2 (a). In a strong field, Fig. 2 (b), the pole surface defects are accompanied by equatorial defect rings at both inner and outer shell surfaces. Contrary to the pole defects (being a consequence of topological constraints) the rings will disappear once the field is switched off. Note that the surface topological charge contribution of each ring is equal to zero and that the pole defects alone account for the total charge that is conserved. — As an example of a field with no axial symmetry consider the $\mathbf{F}_i^2$-type field characterized by D_{2h} symmetry. The defect evolution and the corresponding director fields are shown in Fig. 3. Increasing η, at first the zero-field four-defect line structure is maintained; the defect line positions merely adapt, as required by the field. Then, above a threshold at $\eta \approx 0.04$, a more complex configuration is observed: the four $s = 1/2$ defect lines, valence 4, transform into four $s = -1/2$ defect lines still penetrating the shell, accompanied by four $s = 1$ surface defect pairs, yielding a valence of 8. Note that thanks to defects with negative topological charge that have been introduced in the shell, the overall topological surface defect charge is still conserved. — The structures for other $\mathbf{F}_i^m$, $m \neq 0$, are similar to those reported in Fig. 3, yet oriented in a different way. Linear combinations of $\mathbf{F}_i^m$ and higher order multipoles result in even more complicated and in a way interesting defect patterns. — Notice that in the inhomogeneous field case we have assumed that the nematic shell center coincides with the coordinate system origin. Experimentally, the colloidal particle could be brought in the correct position, e.g., by means of a laser tweezer. Then, after having applied the multipolar field with the desired symmetry, the defect configuration should be suitably stabilized to persist even after the field is turned off.

Concluding, we have shown, using large-scale Monte Carlo simulations, that defect number, strength, and position on a spherical shell can be manipulated by external homogeneous or inhomogeneous fields. In particular, a homogeneous field induces a structural transition from a four half-strength defect line structure to a bipolar structure with two pairs of surface defects on the inner/outer shell poles. Higher-order multipole fields can result in more complicated defect patterns, including negative-strength defect lines. In all cases, however, the total surface defect charge is conserved, as required by the topological constraints. From the point of view of building colloidal assemblies the problem of consolidating the defect structures should clearly be solved. One possibility could be that of performing the ligand attack before switching off the field or of using a polymerization (e.g., photo-initiated) while the multipolar field is acting on the colloidal suspension. Even though this may clearly be challenging from the experimental point of view we believe the possibilities opened by the techniques theoretically demonstrated here are numerous and promising.

[1] D. R. Nelson, Nanoletters **2**, 1125 (2002).
[2] N. D. Mermin, Rev. Mod. Phys. **51**, 647 (1979).
[3] T. C. Lubensky and J. Prost, J. Phys. II **2**, 371 (1992).
[4] S. C. Glotzer and M. J. Solomon, Nature Mater. **6**, 557 (2007).
[5] I. Muševič *et al*, Science **18**, 954 (2006).
[6] G. Zhang *et al*, Angew. Chem. Int. Ed. **44**, 7767 (2005).
[7] J. R. Roan, Phys. Rev. Lett. **96**, 248301 (2006).
[8] Y. S. Cho *et al*, Chem. Mater. **19**, 3183 (2007).
[9] A. Fernández-Nieves *et al*, Phys. Rev. Lett. **92**, 105503 (2004).
[10] A. Fernández-Nieves *et al*, Phys. Rev. Lett. **99**, 157801 (2007).
[11] E. C. Nelson and P. V. Braun, Science **318**, 924 (2007).
[12] M. Huber and H. Stark, Europhys. Lett. **69**, 135 (2005).
[13] P. A. Lebwohl and G. Lasher, Phys. Rev. A **6**, 426 (1972).
[14] C. Chiccoli *et al*, Phys. Rev. Lett. **79**, 4401 (1997).
[15] U. Fabbri and C. Zannoni, Mol. Phys. **58**, 763 (1986).
[16] J. A. Barker and R. O. Watts, Chem. Phys. Lett. **3**, 144 (1969).
[17] see, e.g., D. Frenkel and B. Smit, *Understanding Molecular Simulation: From Algorithms to Applications* (Academic Press, San Diego, 1996).
[18] A. C. Callan-Jones *et al*, Phys. Rev. E **74**, 061701 (2006).
[19] see, e.g., P. M. Chaikin and T. C. Lubensky, *Principles of Condensed Matter Physics* (Cambridge University Press, Cambridge, 1997).
[20] G. E. Volovik and O. D. Lavrentovich, Sov. Phys. JETP **58**, 1159 (1983).
[21] V. Vitelli and D. R. Nelson, Phys. Rev. E **74**, 021711 (2006).
[22] C. Chiccoli *et al*, Phys. Rev. E **62**, 3766 (2000).
[23] K. B. MacAdam and C. S. Hwang, Rev. Sci. Instrum. **74**, 2267 (2003).
[24] see, e.g., J. D. Jackson, *Classical Electrodynamics* (Wiley, New York, 1999).